

Interparticle Distance Variation in Semiconductor Nanoplatelet Stacks

Rebecca T. Graf, Anja Schlosser, Dániel Zámbo, Jakob Schlenkrich, Pascal Rusch, Atasi Chatterjee, Herbert Pfnür, and Nadja C. Bigall*

In the large field of research on nanoplatelets (NPLs), their strong tendency to self-assemble into ordered stacks and the resulting changes in their properties are of great interest. The assembly reveals new characteristics such as the charge carrier transport through the NPL assembly or altered optical properties. In particular, a reduced distance should enhance the charge carrier transport due to higher electronic coupling of neighboring NPLs, and therefore, is the focus of this work. To modify the inter-particle distances, the straightforward method of ligand exchange is applied. Various CdSe and CdSe/CdX (hetero-) NPLs serve as building blocks, which not only display different material combinations but also different types of heterostructures. The surface-to-surface distance between the stacked NPLs can be reduced to below 1 nm, thus, to less than the half compared to assemblies of pristine NPLs. Moreover, for certain NPLs stacking is only enabled by the ligand exchange. To characterize the ligand exchanges and to investigate the influences of the reduced distances, photo-electrochemical measurements, fluorescence spectroscopy, energy dispersive X-ray spectroscopy, nuclear magnetic resonance, and X-ray photoelectron spectroscopy are performed. It is possible to show higher photocurrents for smaller distances, indicating enhanced charge transport ability within those stacks.

precise thickness control resulting from their growth mechanism,^[2] NPLs possess unique optical and electronic properties.^[3,4] In addition to the thickness control at the atomic level, the strong quantum confinement in the thickness direction leads to very narrow emission and absorbance features which are nearly uninfluenced by the lateral extension of the NPLs.^[1,4,5]


Additionally, through lateral and/or axial extension of core NPLs with other materials, it is possible to tune for example the optical properties further by building different heterostructures.^[6–16] By lateral extension, so-called core/crown NPLs are obtained which still possess the same thickness as the corresponding core NPLs.^[6,11,14] Through crown growth, it is possible to form different types of heterostructures depending on the applied materials. CdSe/CdS core/crown NPLs are for example considered as type-I heterostructures, in which the exciton is localized in the core^[8,11] while in CdSe/CdTe core/crown separated charge carriers are present due to the type-II band alignment.^[6,14] Additionally, the kind of growth can influence the type tremendously as can be seen for CdSe/CdS NPLs. As mentioned previously, the CdS crown growth leads to a type-I heterostructure due to the high exciton binding energy.^[8,11] In

1. Introduction

Since their discovery in 2008, colloidal cadmium chalcogenide nanoplatelets (NPLs) or so-called quantum wells opened up a whole new field of research.^[1] Due to the atomically

R. T. Graf, A. Schlosser, D. Zámbo, J. Schlenkrich, P. Rusch, N. C. Bigall
Institute of Physical Chemistry and Electrochemistry
Leibniz Universität Hannover
Callinstraße 3A, 30167 Hanover, Germany
E-mail: nadja.bigall@pci.uni-hannover.de

R. T. Graf, A. Schlosser, D. Zámbo, J. Schlenkrich, P. Rusch,
A. Chatterjee, H. Pfnür, N. C. Bigall
Laboratory of Nano- and Quantum Engineering
Leibniz Universität Hannover
Schneiderberg 39, 30167 Hanover, Germany

 The ORCID identification number(s) for the author(s) of this article can be found under <https://doi.org/10.1002/adfm.202112621>.

© 2022 The Authors. Advanced Functional Materials published by Wiley-VCH GmbH. This is an open access article under the terms of the Creative Commons Attribution-NonCommercial License, which permits use, distribution and reproduction in any medium, provided the original work is properly cited and is not used for commercial purposes.

D. Zámbo
Centre for Energy Research
Institute of Technical Physics and Materials Science
Konkoly-Thege M. str. 29-33., Budapest 1121, Hungary

A. Chatterjee, H. Pfnür
Institute für Festkörperphysik
Leibniz Universität Hannover
Appelstraße 2, 30167 Hanover, Germany

A. Chatterjee
Electrical Quantum Metrology
Physikalisch-Technische Bundesanstalt (PTB)
Bundesallee 100, 38116 Braunschweig, Germany

N. C. Bigall
Cluster of Excellence PhoenixD (Photonics, Optics
and Engineering–Innovation Across Disciplines)
Leibniz Universität Hannover
30167 Hanover, Germany

DOI: 10.1002/adfm.202112621

contrast, the growth of a (thick) CdS shell (growth of CdS in all directions) results in a partial electron delocalization into the shell region and thus, to a quasi-type-II heterostructure.^[7,10,15,17] This opens up manifold possibilities to enhance or alter the properties of the core NPLs, for example, the photoluminescence quantum yield (PLQY), the PL lifetimes, or the charge carrier separation. Due to the high surface-to-volume ratio of NPLs, the surface ligands (type, density) are decisive for the NPL properties.^[18–20]

In general, self-assembly of nanoparticles can link the favorable microscopic characteristics to the macroscopic application and might even generate new properties.^[21–29] So far, NPLs could not only be assembled randomly for example as (cryo-)aerogels^[26,28,30,31] but also possess a high tendency to form ordered stacks.^[24,32–36] Due to their highly anisotropic shape, the self-assembly is favored along the axial direction (in the direction of the thickness). Here, the thickness of four monolayers (4ML) seems to be very beneficial, as small, non-bending NPLs can easily be synthesized in different sizes and aspect ratios (quasi-quadratic, quasi-rectangular).^[20,24,26] One method to stack NPLs is the controlled destabilization of NPLs in solution. Before the destabilization, the NPLs are stabilized in organic solvents (e.g., hexane) through steric ligands with long aliphatic chains (e.g., carboxylic acids: oleic acid). A slow injection of an antisolvent to a NPL dispersion leads to the formation of assembled NPLs with intercalating ligands. This assembly takes place due to long-range attractive van-der-Waals forces between the NPLs as 2D objects and a simultaneous reduction of the contact area of the ligands with the antisolvent (e.g., polar solvents: ethanol (EtOH), acetonitrile (ACN)).^[19,32–35] Resulting from the anisotropic shape of the NPLs, the assembly occurs in the thickness direction of the NPL which leads to NPL stacks. The initial repulsive forces between the ligands turn into attractive forces as a result of the changed polarity of the solvent which, in turn leads to ligand intercalation and thus a minimalization of the contact area with the antisolvent.^[19,32–35] Hence, the chosen surface ligands play a crucial role and can influence the stacking behavior tremendously. Tailoring the ligand types and amounts can yield staircase-like stacks in which the NPLs are twisted^[20] or stacks comprised of NPLs with nearly the same orientation.^[19] A different method to self-assemble NPLs is the arrangement at a liquid layer interface exploiting the interaction potential between NPLs and the solvent. There, the kinetic control (fast evaporation of solvents) leads to NPLs laying flat (face-down) on a substrate while the thermodynamic control (slow solvent evaporation) results in stacked (edge-up) assemblies on the substrate which is energetically favored but requires time to arrange.^[36]

The ordered assembly leads to new or unnoticed features of the NPLs such as the appearance of a phonon line at low temperatures^[32] or the polarization of light through macroscopic CdSe NPL stack needles.^[34] Furthermore, the exciton transfer between NPLs with center-to-center distances of 4.29 nm was characterized via PL lifetime measurements.^[33] It was shown, that the exciton transfer happens through resonant non-radiative energy transfer processes between the same emitters called homo-Förster resonance energy transfer (FRET).^[33] Moreover, the charge carrier transport through CdSe stacks could be verified directly by photo-electrochemical measurements.^[24] Just

recently it was shown that the charge carrier dynamics is altered by the assembly. While excitons are present in dispersed NPLs, the presence of separated charge carriers could be verified by THz spectroscopy.^[36] The transition from excitons to separated charge carriers was ascribed to the high electronic coupling of neighboring NPLs if assembled with small distances.^[36]

In previous reports, the NPL–NPL distance within the stacks and its possible influence on the optical and photo-electrochemical properties was hardly addressed. Considering the fact that smaller distances should greatly enhance charge carrier tunneling due to larger electronic wavefunction overlap of neighboring NPLs,^[36] a decrease of the NPL–NPL distance might pave the way toward future applications of NPL assemblies for example, as (photo)transistors,^[37–40] photoconductors,^[40] sensors,^[26] for photodetection,^[41–43] in solar cells, or as light emitting diodes.^[44] To manipulate the NPL–NPL distance, ligand exchange is a straightforward method since the NPL ligands mainly govern the distance in the stacks.^[24]

The present work focuses on the minimization of the NPL–NPL distance to enable enhanced electronic transport within the stacks. A ligand exchange method is introduced to replace the native long chain carboxylic acid based ligands by amine ligands of varying length. The exchange is assisted by the addition of different amounts CdBr₂. Afterward, the ligand exchanged NPLs are employed in the assembly of NPL stacks with ultra small NPL–NPL distances. This method is also extended to different NPL materials and heterostructure types (CdSe/CdS-core/crown type-I, CdSe/CdTe core/crown type-II, CdSe/CdS core/shell quasi-type-II). Furthermore, a polymer encapsulation step which was previously shown to not only stabilize the formed stacks mechanically and enable the phase transfer to aqueous solutions but also to further reduce the NPL distance through depletion attraction forces,^[22,24] is employed. The resulting polymer encapsulated NPL stacks (called PENS in the following) are characterized with regard to their optoelectronic properties by spectroscopy and photo-electrochemistry allowing conclusions on the charge carrier transport within the PENS.

2. Results and Discussion

2.1. Synthesis and Characterization of NPL Building Blocks

At first, CdSe core NPLs with a thickness of 4ML and an emission maximum at 514 nm (full-width-at-half-maximum (FWHM) 10.8 nm) following already published procedures were synthesized.^[24,34] These NPLs then either served as seeds for the growth of different core/crown and core/shell NPLs or were directly applied in the synthesis of PENS (**Figure 1**).

Detailed characterization results of all synthesized NPLs are available in the Supporting Information. In **Figure 2a–d**, TEM images of the different (hetero-)NPLs are shown. All NPLs are characterized by a nearly ideal quasi-quadratic shape and therefore equal edge lengths which supports the formation of straight, untwisted PENS later on. However, the absolute edge lengths as well as the optical properties of the NPLs depend on the modification type. The UV–vis and PL emission and excitation spectra of the as-synthesized NPL solutions are shown in **Figure 2e–h**. Through CdS and CdTe crown

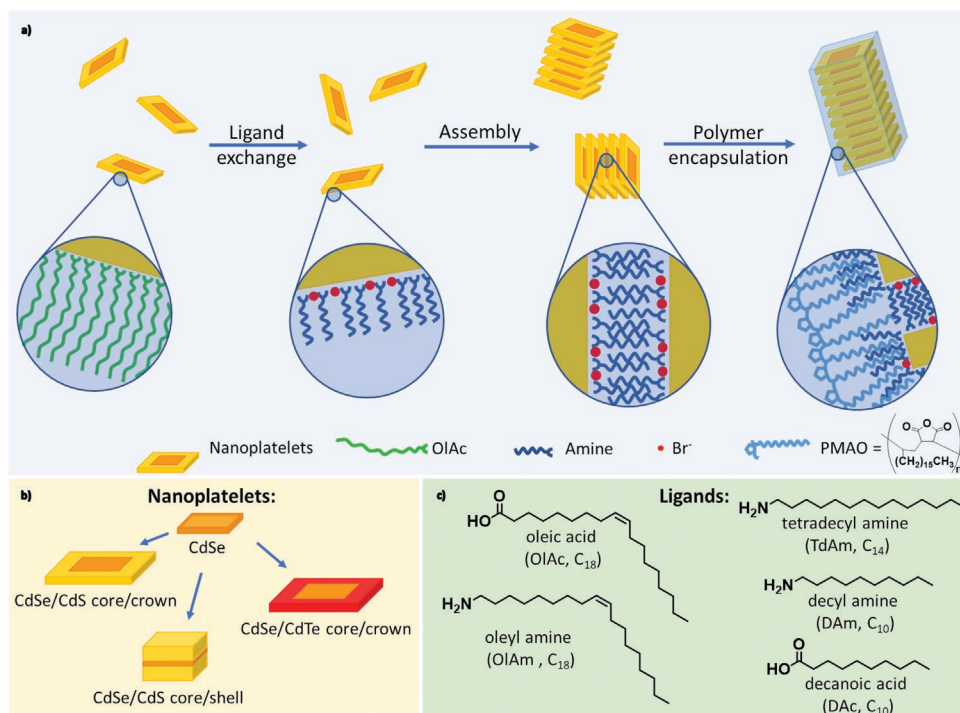


Figure 1. a) Scheme of the preparation process of polymer encapsulated nanoplatelet stacks (PENS) with tunable NPL–NPL distances. At first, the native oleic acid/oleate ligands are exchanged by CdBr₂ and aliphatic amines. After dissolution of the Br-Amine capped NPLs in THF, acetonitrile is added in order to trigger the assembly of the NPLs into small stacks. By the addition of a solution of poly(maleic anhydride-*alt*-1-octadecene) (PMAO), the pre-formed stacks are stabilized and encapsulated with a polymer shell forming PENS. The chosen NPLs b) are CdSe core-only, CdSe/CdS core/crown, CdSe/CdTe core/crown and CdSe/CdS core/shell NPLs. c) Ligands prior (OIAc) and after the ligand exchanges (OIAm, TdAm, DAm, and DAC).

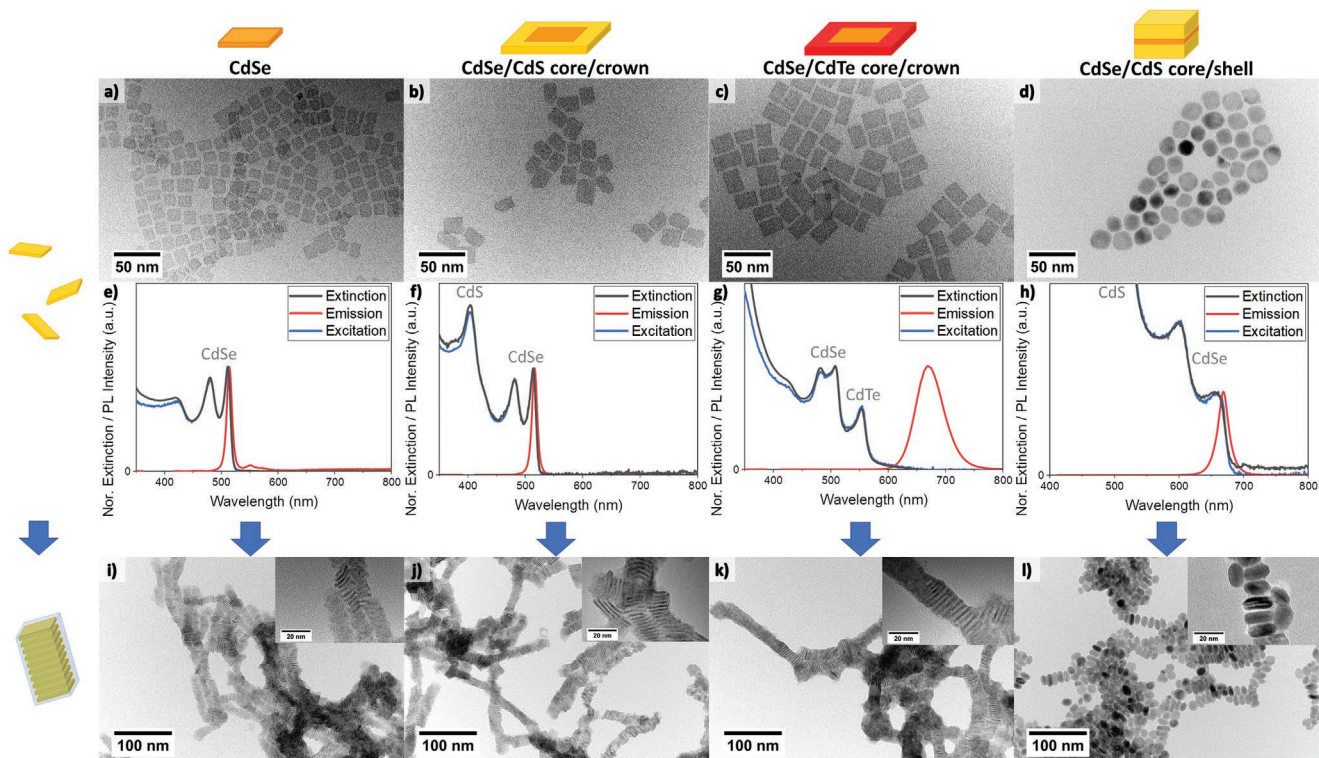


Figure 2. TEM micrographs of the synthesized NPLs: CdSe (a), CdSe/CdS core/crown (b), CdSe/CdTe core/crown (c), and CdSe/CdS core/shell NPLs (d). Corresponding extinction (black), emission (red), and excitation spectra (blue) of NPL dispersions in hexane (e–h). With the developed procedure, PENS of all shown NPLs are synthesizable (i–l, exchanged with decylamine and 10 : 1 Br to surface Cd atoms, later referred to as DAm and 10-fold Br).

growth, (quasi-)type-I and type-II heterostructures are created, respectively.^[6,8,11] In a combined CdSe/CdTe heterostructure, the valence band of CdTe is located in the band gap of CdSe which can lead to photo-induced charge separation. Hence, CdSe/CdTe core/crown NPLs are characterized by remarkably higher emission wavelengths than the corresponding CdSe cores, as radiative recombination takes place across the semiconductor interface. A similar emission shift is observed for CdSe/CdS core/shell NPLs, which is caused by the increased NPL thickness and therewith reduced quantum confinement leading to a quasi-type-II heterostructure.^[7,9]

2.2. Synthesis of Polymer Encapsulated Nanoplatelet Stacks (PENS) and Manipulation of the NPL–NPL Distance

Independent of the NPL thickness and lateral dimensions, PENS could be obtained from all shown NPL types (Figure 2i–l). This demonstrates the versatility of the applied assembly technique, which will be explained more in depth in the following. The applied protocol for the assembly of NPLs into PENS is illustrated in Figure 1a.

The procedure was developed based on our previous method for the synthesis of CdSe NPL/polymer fibers (here called PENS).^[24] By introduction of an additional ligand exchange step, not only the versatility of the method was improved but also the NPL–NPL distances within the PENS could be drastically reduced (CdSe core NPLs: from 2.1 to 0.8 nm).

Directly after the synthesis, the surfaces of the core-only and core/crown NPLs are passivated with long-chain carboxylic acids (myristic acid and oleic acid) and tri-*n*-octylphosphine (TOP) (only core/crown NPLs). If the NPLs are assembled into stacks, the ligands remain on the NPL surfaces, however, they are able to intercalate between the ligands of the neighboring NPLs.^[33,34] Hence, the NPL–NPL distance inside the PENS is mainly governed by two factors: the (chain) length of the surface ligands and the packing density of the ligands on the NPL surface. In addition, the application of a polymer was observed to further reduce the NPL–NPL distance in the PENS to a certain extent.^[24] In order to manipulate the NPL–NPL distances inside the PENS, the native ligands of the NPLs were exchanged to CdBr₂ and aliphatic amines following a method by Dufour et al.^[18] In contrast to other ligand exchanges performed for NPLs,^[45,46] the PLQY of the NPLs could be retained or even improved by the application of this protocol. The ligand-exchanged NPLs were subsequently transferred to tetrahydrofuran (THF) to prevent agglomeration of the polymer in the polymer encapsulation step.^[22] In order to trigger the self-assembly of the NPLs into stacks, acetonitrile was added to the NPL-THF solution. The stack were further stabilized by addition of an amphiphilic polymer (poly(maleic anhydride-*alt*-1-octadecene), PMAO) containing non-polar aliphatic chains and cyclic anhydride groups which was used for other nanoparticle assemblies in the past.^[22,24,47] While the aliphatic chains are able to interact with the non-polar ligands of the NPLs, the anhydride rings face the solution and facilitate the water transfer of the PENS in the final step.

By the described procedure, multiple types of hetero-NPLs could be transformed into PENS. Especially CdSe, CdSe/CdTe core/crown, and CdSe/CdS core/shell NPLs only hardly formed

ordered PENS if the original procedure (without ligand exchange) was applied. Instead, with the modified procedure long ordered PENS (up to 800 nm for CdSe/CdS core/crown) could be obtained for all investigated NPLs (Figures S11–S13, Supporting Information). In the case of CdSe/CdS core/shell NPLs with native ligands, only negligible amounts of NPLs could be assembled into stacks. This can be explained by the reduced anisotropy after (thick-)shell growth and the rather ellipsoidal shape of the core/shell NPLs, which both lead to a drastically reduced ligand intercalation possibility. In this case, the ligand exchange facilitates the stacking, possibly due to the formation of larger distances between the steric amine ligands leading to better intercalation of the ligands as explained in Section 2.2.3. Out of CdSe/CdS core/crown NPLs, PENS could be obtained both with and without ligand exchange. Hence, these NPLs were selected for further studies about the influences on the NPL–NPL distance in the PENS.

2.2.1. Influence of the Ligand Length on the Inter-NPL Distance in PENS

To study the influence of the amine chain length on the NPL–NPL distance, decyl amine (DAm, C₁₀, completely stretched 1.4 nm, calculated by the Tanford formula,^[48] Equation (S1), Supporting Information), tetradecyl amine (TdAm, C₁₄, 1.9 nm) and oleyl amine (OlAm, C₁₈ with one double bond, 2.5 nm^[32]) were used for the exchange of the surface ligands of CdSe/CdS core/crown NPLs while the amount of CdBr₂ was kept constant at the 10-fold amount of bromide ions in relation to the quantity of Cd surface atoms (samples: DAm and 10-fold Br, TdAm and 10-fold Br, OlAm 10-fold Br).^[18] The progress of the ligand exchange can easily be monitored by PL spectroscopy due to the shifting emission maximum when bromide binds to the surface^[18] (Figure S14c,d, Supporting Information). Judging from the development of the emission maximum, the ligand exchange was observed to proceed at approximately the same rate independent of the amine length. In all cases, the emission maximum stabilized at 531 to 533 nm after 24 h of exchange time. In the UV–vis spectra of the differently capped NPLs recorded after this time period (Figure S6, Supporting Information), also no significant differences in the positions of the absorbance maxima are visible. Photoluminescence quantum yield (PLQY) measurements revealed that the PLQY of oleate capped NPLs (pristine) is slightly improved by the ligand exchange with DAm and 10-fold Br and TdAm and 10-fold Br (an increase of 1.1% and 1.9%, respectively; Figure S7, Supporting Information). For OlAm and 10-fold Br capped NPLs, in contrast, a significantly stronger increase of the PLQY of 14.9% (to 57.3%) was recorded, probably caused by a better shielding of the NPL surface through the longer OlAm molecules. Due to the low curvature of the NPL surfaces, the ligand density depends on the attractive forces between the ligands and therefore increases with the ligand length.^[49] Hence, the diffusion of solvent molecules to the NPL surface and the interaction of both is diminished.

In order to obtain PENS, the amine-Br capped NPLs were then transferred to THF, destabilized (assembled to stacks) and surrounded by poly(maleic anhydride-*alt*-1-octadecene) (PMAO) forming polymer encapsulated NPL stacks (PENS) (Figure 1a).

The dispersion of the amine-Br capped CdSe/CdS core/crown NPLs in THF led to a further reduction of the NPL PLQY by 8% to 14%, depending on the applied amine. The decrease in the PLQY can be explained by the comparably high polarity of THF which facilitates the interaction between the solvent molecules and the NPL surface.^[50,51] After the destabilization and polymer encapsulation, ordered fiber-like structures could only be obtained in case of TdAm and 10-fold Br and DAm and 10-fold Br capped NPLs (Figure S8c,d, Supporting Information). If OlAm and 10-fold Br capped NPLs were applied, PENS were still formed, but no elongated structures and polymer shells are visible (probably because of the long angled ligands or a higher coverage with steric ligands, see Figure S8b, Supporting Information).

The influence of the amine chain length on the NPL–NPL distance can be derived from the higher magnification TEM images shown in Figure 3. In the images, the stacked NPLs appear as dark stripes as they are standing on their edges, whereas the surrounding polymer is only barely visible due to the low contrast differences with the background. The NPLs inside the PENS are well-ordered and the distance between the single NPLs decreases with decreasing chain length (for exact values see Table 1). For the shortest applied amine, DAm, C₁₀, the smallest surface-to-surface distance between the NPLs of (0.92 ± 0.22) nm was determined, which is even significantly lower than the calculated length of a single DAM molecule (1.4 nm). This implies, that the ligands of neighboring NPLs are intercalating between each other and moreover, that the chains of the amine ligands are not fully stretched. This compression of the ligands is likely related to two factors: 1) the application of the polymer, as it was already demonstrated to introduce an additional entropic force (depletion attraction) onto the PENS^[24] and 2) the reduced density of steric surface ligand (amine) after the ligand exchange. The latter factor is corroborated by the fact, that the NPL–NPL distance inside the PENS is significantly decreased if OlAm (C₁₈) and 10-fold Br capped NPLs instead of OlAc (C₁₈) capped NPLs are applied, although the chain length of the ligands should be comparable in both cases (2.5 nm^[32]). To verify the latter hypothesis (2) the ligand exchange with amine and CdBr₂ was investigated in more detail.

In summary, the inter-NPL distance could be reduced by applying a ligand exchange with (shorter chained) amines and CdBr₂. As expected, a direct correlation between ligand length and NPL–NPL distance was observed. Interestingly, significantly lower distances than the calculated lengths of the (fully stretched) amine ligands were measured. Especially the application of CdBr₂ in the ligand exchange proved to be of high importance for the inter-NPL distance and will be discussed in the next section.

2.2.2. Influence of the CdBr₂ Amount on the Inter-NPL Distance in the PENS

The NPL–NPL distance inside the PENS was observed to be sensitive to the amount of CdBr₂ applied in the ligand exchange. While the amount of DAm was kept constant, the ratio of the amount of Br to the quantity of surface Cd atoms was varied between 1:1 and 20:1 (samples denoted as DAm and

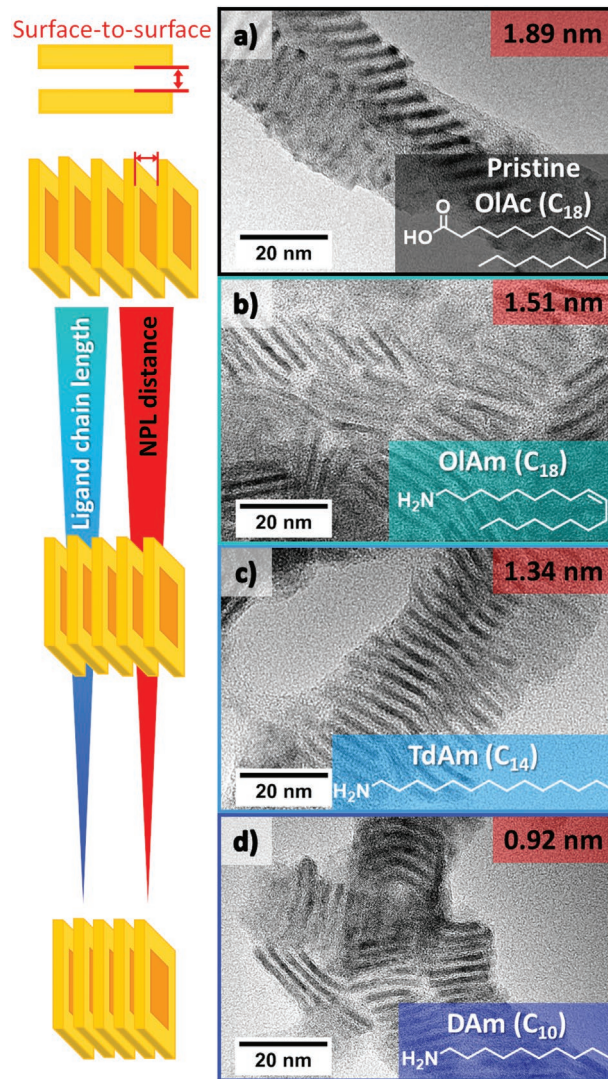


Figure 3. TEM micrographs of polymer encapsulated nanoplatelet stacks (PENS) without (a) and with ligand exchanges (b–d). The NPLs inside the PENS are capped by the following ligands: without a ligand exchange: a) oleic acid (pristine NPLs) and after ligand exchanges with CdBr₂ and different amines: b) oleyl amine (OlAm, C₁₈), c) tetradecyl amine (TdAm, C₁₄), and d) decyl amine (DAm, C₁₀). The CdBr₂ amount was constant at a 10-fold excess of bromide ions to Cd surface atoms. The surface-to-surface NPL–NPL distance (red) was observed to decrease with decreasing chain length of the applied amine.

1-fold Br and DAm and 20-fold Br, respectively). One ligand exchange reaction was moreover performed without the addition of any CdBr₂, denoted as DAm (and no Br).

The emission spectra recorded during the ligand exchange with DAm and CdBr₂ (Figure S9a,b, Supporting Information) show, that the exchange rate directly depends on the amount of CdBr₂ applied. However, no significant differences in the position of the emission maximum after 24 h were recorded, even though the exchange was observed to proceed faster if high amounts of CdBr₂ were added. If no CdBr₂ was present, the emission was irreversibly quenched after the addition of DAm. The extinction spectra are discussed in the Supporting Information. The PLQY of the ligand exchanged NPLs was observed to increase with

Table 1. Surface-to-surface distances of stacked CdSe/CdS core/crown NPLs after different ligand exchanges measured by TEM, with number of measurements n .

NPL	Inter-NPL distance [nm]	n
OlAc (pristine)	1.89 ± 0.27	117
DAm and 10-fold Br	0.92 ± 0.22	115
TdAm and 10-fold Br	1.34 ± 0.20	
OlAm and 10-fold Br	1.51 ± 0.31	104
DAC	1.64 ± 0.31	82
DAm and no Br	1.69 ± 0.28	64
DAm and 1-fold Br	1.20 ± 0.22	116
DAm and 2.5-fold Br	1.09 ± 0.22	60
DAm and 10-fold Br	0.92 ± 0.22	115
DAm and 20-fold Br	0.90 ± 0.18	92

increasing CdBr₂ amount from 8.1% to 31.9% (in THF) for DAm and 1-fold Br to 20-fold Br, respectively. Figure 4 shows TEM images of the corresponding PENS, in Table 1 the measured NPL–NPL distances inside the PENS are collected. Independent of the CdBr₂ amount applied in the ligand exchange, elongated PENS consisting of stacked NPLs encapsulated with a polymer shell were obtained. Analogue experiments with DAm and CdCl₂ are shown in Section S2.7, Supporting Information to analyze whether CdBr₂ could be substituted by other halides. Thereby, the exchange with chloride lead to partially similar results, forming PENS with decreased inter-NPL distances while the stability of the NPLs in THF was rapidly decreased, leading to inhomogeneous polymer shells (for further details see Supporting Information).

The NPL–NPL distance inside the DAm and CdBr₂ exchanged PENS was observed to decrease with increasing CdBr₂ amount. To interpret these observations, the different types of surface ligands need to be considered, which are visualized schematically in Figure 5d. Due to the structure of the NPLs, 4ML thick NPLs consist of four layers of Se and five layers of Cd and contain a Cd layer at the top and bottom. Hence, they possess a formal positive charge, which can be compensated by X-type surface ligands (Figure 5d, red), for example, carboxylate ions. If bound to the surface of the NPLs, a certain fraction of the oleic acid molecules should consequently be deprotonated as oleate ions. The native X- and L-type ligands can only be removed completely by application of a high excess of new charge-compensating (X-type) ligands. After the ligand exchange with CdBr₂ and OlAm, Dufour et al., postulate the formation of a bromide ion (Br⁻) layer at the Cd-surface, with Br⁻ acting as X-type ligand.^[18,52] Furthermore, they suggest that the amines are bound to the bromide layer via H-bonds between the Br⁻ and amine group (Cd–Br⋯H–NHR). In general, there are also other possibilities how the applied ligands can interact with the NPLs: 1) the amine can directly bind to the NPL as an L-type ligand (Cd⋯NH₂R), similar to oleic acid (Figure 5d, violet), 2) CdBr₂ can heal Cd surface vacancies through insertion of the Cd into the vacancy, and 3) CdBr₂ can act as Z-type ligand being bound to chalcogenide atoms at the edges while passivating those (Figure 5d, cyan).^[52] The latter two can be explanations for the increasing PLQY after the ligand exchange.

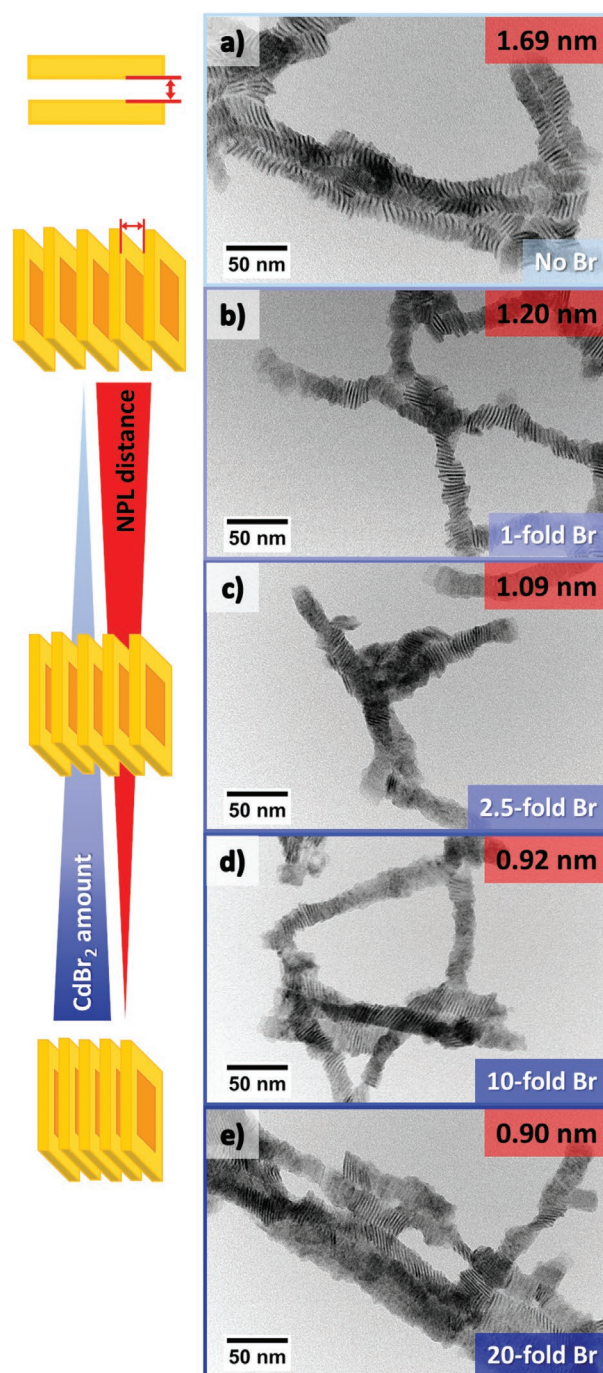


Figure 4. TEM images of polymer encapsulated NPL stacks synthesized from CdSe/CdS core/crown NPLs with different ligand shell compositions. In the ligand exchanges which were performed prior to the fiber assembly, different amounts of CdBr₂ in addition to a constant amount of decyl amine (DAm) were applied: a) no Br, b) 1-fold amount, c) 2.5-fold amount, d) 10-fold amount, and e) 20-fold amount of the bromide ions with respect to the quantity of Cd surface atoms of the NPLs. The surface-to-surface NPL–NPL distance (red) was observed to decrease with an increasing amount of CdBr₂ in the ligand exchange (light to dark blue).

The structure of the ligand shell as described by Dufour et al., can only hardly explain the observed dependence of the NPL–NPL distance on the CdBr₂ amount. In this work, the

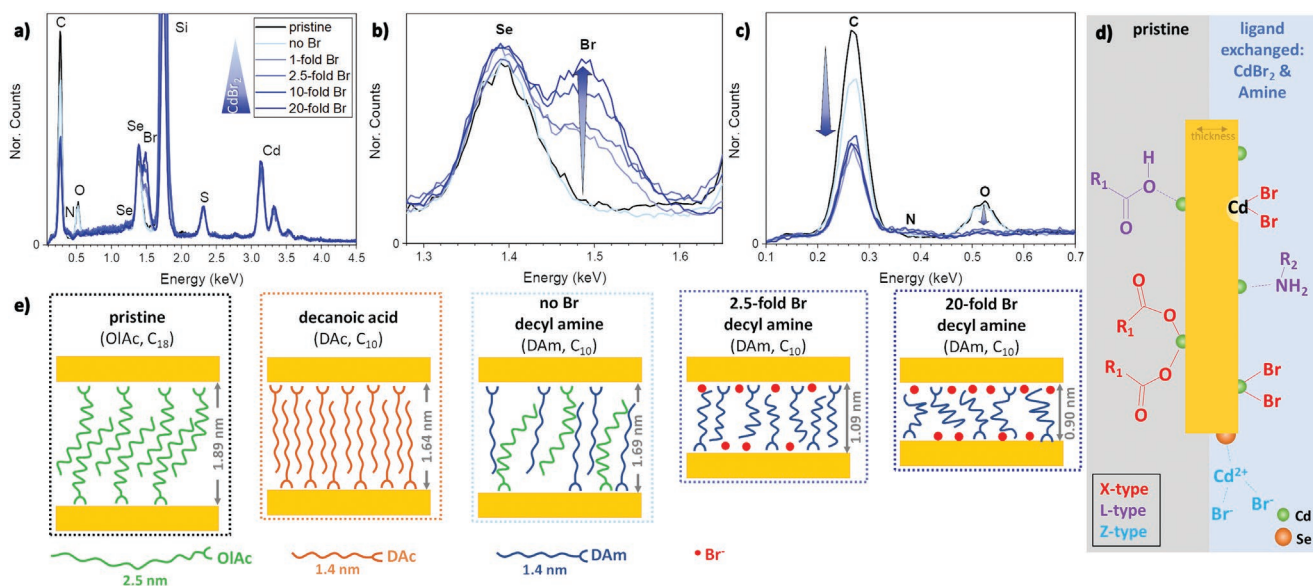


Figure 5. EDX spectra of CdSe/CdS NPLs with different ligand shell compositions (a–c). In the ligand exchanges, different amounts of CdBr₂ in addition to a constant DAM amount were applied. The regions of Se–Br (b) and C–N–O (c), are displayed in higher magnification. The counts were normalized to the sulfur signal for better comparison. d) Scheme of different binding types before (gray, left) and after the ligand exchanges with CdBr₂ and amines (blue, right). While the acid and the amine can act as L-type ligands (violet), the carboxylate and bromide ions are X-type (red) and the CdBr₂ can bind as Z-type ligands (cyan) or heal Cd vacancies. In the scheme, the surface Cd atoms are symbolized by green and the chalcogenide atoms (Se, S) by orange circles. e) Schematic visualization of the resulting ligand coverage after certain ligand exchanges showing the resulting inter-NPL distances in the PENS.

amount of amine was kept constant at high excess, while the CdBr₂ amount was varied between 1:1 and 20:1 Br to Cd surface atoms. Hence, the formation of a complete Br layer should be possible for all CdBr₂ amounts, so no remarkable influence on the NPL–NPL distance is expected. In contrary, we observed a decrease in the NPL–NPL distance by 30% by applying the 20-fold amount of CdBr₂. This effect was not only observed for CdSe/CdS core/crown NPLs, but also for CdSe core-only NPLs (Table S3, Supporting Information).

For comparison, a ligand exchange with decanoic acid (DAC, C₁₀) was performed. After stacking and polymer encapsulation, PENS with lower NPL–NPL distances than in case of pristine NPLs were obtained, due to the shorter chain length of decanoic acid compared to oleic acid (C₁₈ → C₁₀, Figure 5e). In PENS containing NPLs with only the corresponding amine ligand (DAM, C₁₀ and no Br), slightly larger distances than that of the decanoic acid PENS were observed, which might be related to incomplete removal of the native ligands by the L-type amines. However, as soon as cadmium bromide is added in the ligand exchange with amine (e.g., DAM and 1-fold Br) the opposite is observed, as PENS with amine and CdBr₂ capped NPLs are showing smaller distances than the corresponding acid ones consisting of DAC-capped NPLs. This leads to the assumption, that the steric ligands (the alkyl chains) have to be less densely packed when CdBr₂ is present in the ligand exchange. Hence, they are able to interpenetrate further into the ligand shell of the neighboring NPL and experience a stronger compression (Figure 5e). One explanation for the decreasing distance with increasing CdBr₂ amount would be a competition mechanism between the Br[−] and amine ligands for surface sites. By this, a mixed shell of Br[−] bound as X-type ligand and amine bound as L-type ligand would be formed. This, in turn, will lead to a

lower amount of amine on the surface and therefore larger distances between the steric amines, which will further increase with increasing bromide content at the NPL surface. Hence, the amine chains can be compressed more easily and the NPL–NPL distance in the PENS can be decreased far below the actual ligand length (Figure 5e). This theory would explain our findings satisfyingly.

To summarize, the inter-NPL distance depends on the CdBr₂ amount used in the ligand exchange prior to the assembly. The distance was observed to decrease with an increasing CdBr₂ amount, far below the inter-NPL distances of the samples exchanged with the corresponding acid or amine without CdBr₂. A competition mechanism between bromide ions and amine ligands for surface sites seems to be a good explanation for these findings, leading to larger distances between the steric alkyl chains of the ligands, resulting in enhanced intercalation of less stretched ligands.

2.2.3. Characterization of the Ligand Shell

To understand the distance dependency and to get more insights into the ligand exchanges, energy dispersive X-ray spectroscopy (SEM-EDX), X-ray photoelectron spectroscopy (XPS), and nuclear magnetic resonance (NMR) of the ligand exchanged NPLs were performed. The composition of the ligand shell after the ligand exchange was characterized by means of different analytical techniques. SEM-EDX of different ligand exchanged NPLs revealed an increasing bromide signal with increasing CdBr₂ excess during the ligand exchange (Figure 5a,b, spectra normalized to the sulfur amount for better comparison).

This result verifies the presence of different bromide amounts in the samples, even though at least 1 bromide ion per cadmium surface atom (DAm and 1-fold Br sample) was introduced during ligand exchange. Hence, an incomplete Br⁻ layer at the NPL surfaces is formed at low bromide content, which is in good agreement with our proposed competition between Br⁻ and amine ligands.

This assumption is furthermore confirmed by the XPS results (Figure S22, Supporting Information). The Br 3d signals 3d_{5/2} (69.9 eV, Figure S22e,f, Supporting Information) and 3d_{3/2} are in accordance with the known binding energy for CdBr₂.^[53] The intensity of the Br signal increases with increasing CdBr₂ amount used in the ligand exchanges while PENS without DAm (and no Br) and pristine PENS show, as expected, no Br signal. Furthermore, differences in the C1s region (Figure S22a,b, Supporting Information) of the differently capped NPLs are observed. The characteristic XPS signals for C–C/C–H (284.4 eV), C=O (288.2 eV), and C–O (286.5 eV) are visible for the pristine and DAm (and no Br) NPLs and belong to the oleic acid or the carboxylate.^[53] The C=O signal decreases rapidly if CdBr₂ is present in the ligand exchange, while a C–O/C–H shoulder is still visible for low amounts of CdBr₂. As the signal originating from C–N groups is also located at a similar energy, it is difficult to distinguish between C–O and C–N, hence oleic acid or amine species.^[53,54] Those findings for DAm (and no Br) match well with the EDX and TGA data and our theory of incomplete ligand exchange without CdBr₂ due to missing X-type ligands (Figure 5e). In the EDX, an oxygen signal is only measurable for the pristine and DAm (and no Br) sample. This can be assigned to the carboxylic oxygen atoms in OlAc, thus, oleic acid is still present in the DAm (and no Br) sample.

To prove that these residual OlAc molecules are attached to the NPL surface in addition to OlAm, NMR spectroscopy was performed. By means of this method, it is possible to distinguish between bound and free ligands. For ligands bound to the NPL surface, the intra-molecular rotation around all types of C–C bonds is hindered. Hence, H atoms attached to the same C atom are not equivalent any more which leads to a broadening of the corresponding signal in the ¹H spectrum. In case of OlAc containing samples, the signal of vinyl H atoms is often used for evaluation. Figure S24, Supporting Information, shows the ¹H NMR spectra of pure oleic acid and different NPL samples between δ = 5.2 ppm and δ = 5.6 ppm. A signal in this region is only present for pure oleic acid, pristine NPLs, and DAm (and no Br) NPLs. In the latter two cases, the signal consists of a broadened and a sharp part (at lower δ). This implies, that OlAc molecules are bound to the NPL surface in both samples as well as that a certain amount of free OlAc is present. However, a determination of the OlAc:DAm ratio cannot be performed due to overlapping signals and solvent residues.

In conclusion, it was possible to show that the bromide content of the NPLs depends on the amount of CdBr₂ applied in the ligand exchange. Furthermore, it could be verified that OlAc can only be removed completely from the NPL surface if bromide is present. These results confirm the previously described competition between bromide and amine for surface sites which results in decreasing inter-NPL distances in the PENS with increasing CdBr₂ amount. Nevertheless, neither an absolute quantification of the amine/nitrogen nor a determination

of the N:Br ratio was possible by the applied methods. A more detailed evaluation of all characterization results is given in the Supporting Information (Section S3, Supporting Information).

2.3. Characterization of the Electronic Transport

To gain insights into the charge carrier transport inside the PENS, time-resolved photoluminescence spectroscopy and different photo-electrochemical techniques were applied. Before interpreting the acquired data, the different possible charge transfer mechanisms need to be discussed. In general, charge carriers can move across the stack in different ways: 1) as separated charge carriers^[36] or 2) as complete excitons via Förster resonance energy transfer (FRET).^[33] For micrometer-scale CdSe NPL assemblies, Guzelurk et al., reported exciton transfer through homo-FRET within the stacks between neighboring NPLs with a surface-to-surface distance of 3.09 nm (4.29 nm center-to-center minus 1.2 nm NPL thickness).^[33] They calculated a Förster radius of ≈13 nm with a NPL-to-NPL hopping time of around 3 ps in their system. Their samples showed shorter PL lifetimes with increasing stack length since a single non-emitting NPL inside a stack facilitates a fast recombination in case of homo-FRET.^[33]

In contrast, Momper et al., showed the generation of separate charge carriers via terahertz (THz) spectroscopy, if dispersed CdSe NPL were assembled into the edge-up (stacked) configuration with a surface-to-surface NPL distance of 2.5 nm.^[36] Here, the change from excitons (in dispersed NPLs) to free charge carriers was explained by the enhanced electronic coupling of neighboring NPL due to wave function overlap which highly depends on the inter-NPL distance and the total NPL–NPL interaction area.^[36,55] In addition to THz spectroscopy, they applied PL emission spectroscopy and noticed a significant broadening in the assembled sample (FWHM 10.14 nm) compared to a dispersion of non-assembled CdSe NPLs (FWHM 8.08 nm) as well as a bathochromic shift (2.45 nm) caused by enhanced inter-NPL coupling.^[36,56]

Judging from the observed NPL–NPL distances, our system is closest to the latter system by Momper et al. Furthermore, smaller distances and ordered stacks should strongly enhance the NPL–NPL coupling and thus, the charge carrier separation as previously reported.^[36,55] In addition, a large broadening of the PL emission of the PENS (up to 29 nm) compared to the respective NPL dispersions (Figure S10, Supporting Information) was observed. This is in line with the measured broadening (2 nm^[36]) due to enhanced NPL-coupling explained by Momper et al., while no broadening was reported for homo-FRET.^[33] The even much stronger PL broadening could be attributed to substantially smaller NPL–NPL distances (2.5 nm vs 1.9...) leading to higher inter-NPL coupling.^[55,56] Furthermore, the NPLs possess elongated PL lifetimes (Figure S34, Supporting Information) when assembled into PENS, most probably resulting from separated and more delocalized charge carriers in the stacks. If CdSe/CdS core/crown NPLs are applied as building blocks, the hole is presumably trapped in the CdSe core (due to the higher valence band of the CdSe) while the electron can be transferred through the stack (considering the small conduction band differences in CdSe and CdS), resulting in elongated lifetimes. In

conclusion, all findings strongly imply the existence of separated charge carriers in PENS, which might be transferred through electron tunneling, while excitons exist in dispersed NPLs (due to the high exciton binding energy) analogue to the work of Momper et al.

Independent of the kind of transport, a smaller distance should be advantageous for the transfer, comparable to a smaller barrier which needs to be overcome. Thus, higher CdBr_2 amounts in the ligand exchange are indirectly, through the dependency of the NPL distance, beneficial for a better transport. In order to monitor any influences of the NPL–NPL distance variation on the (photo)electrochemical properties, that is, the charge carrier transport, different photo-electrochemical (PEC) measurements were performed. Linear sweep voltammetry (LSV), intensity modulated photocurrent spectroscopy (IMPS) and impedance spectroscopy were performed on different ligand exchanged PENS. Previously, our group demonstrated that LSV and IMPS are powerful tools to study the electrical transport through CdSe PENS.^[24] Prior to the PEC characterizations, the PENS were immobilized on indium tin oxide (ITO)-coated glass slides via (3-mercaptopropyl)trimethoxysilane (MPTMS, scanning electron microscopy images can be seen in Figure S32, Supporting Information). The applied immobilization process resulted in thick films on the ITO surface, with a high probability for a random distribution of the PENS, meaning some PENS standing in different angles on the surface and some laying flat. During an LSV measurement, a blue LED (468 nm) is pulsed with alternating on–off cycles of 12.5 s each while the bias potential is modulated from –600 to 300 mV. At low bias potentials, negative photocurrents are measurable for all samples (Figure 6a). This can be explained by the formation of excited electrons and holes through light irradiation and the dominance of certain charge carrier transfer processes. In case of negative photocurrents, excited electrons are transferred from the semiconductor to the aqueous solution and H_2 is generated by reduction of protons. Simultaneously,

the photogenerated hole is quenched by electrons from the electrode (Figure 6c green arrows). With increasing bias potential, positive photocurrents are measurable for all samples (Figure 6a). Positive photocurrents are generated, if photo-excited electrons are transferred from the NPLs to the electrode, while the electrolyte (Na_2SO_3) reacts as hole scavenger (Figure 6c, red arrows). The transition from negative to positive photocurrent switching point (PEPS), is located at different bias potentials for the different samples. It should be noted that the measured photocurrent is the net value of anodic and cathodic processes taking place at the same time and hence the dominant processes herein.^[25] The position of the PEPS has been shown to be influenced by different factors like the pH and the amount of surface traps, thus, different surface ligand coverage.^[25,26] For the different NPL/polymer samples, the PEPS (Figure 6a, arrows) seems to be partially dependent on the CdBr_2 amount in the ligand exchange. More CdBr_2 leads to a PEPS located at lower bias potentials. This observation could be attributed enhanced electron transport to the electrode (less driving force) due to the smaller NPL–NPL distances in case of higher CdBr_2 amounts. Furthermore, the overall photocurrent density was observed to increase quite rapidly in the same direction (increasing CdBr_2 amount). This value can be directly compared for the different PENS, as the same material amount was immobilized on the electrodes in all cases. An increasing photocurrent density might in general explained by either generation of more photoexcited electrons or enhanced/more efficient charge carrier transport to the electrode. The amount of generated charge carriers will be nearly similar for all PENS samples, as their building blocks only differ slightly in the composition of their ligand shell (amount of organic and inorganic ligands). However, the efficiency of the charge carrier transport through the stack will be strongly altered by changes in the interparticle distance, hence it will be affected by the applied ligand exchange. When compared to an electrode coated with a (sub-)monolayer

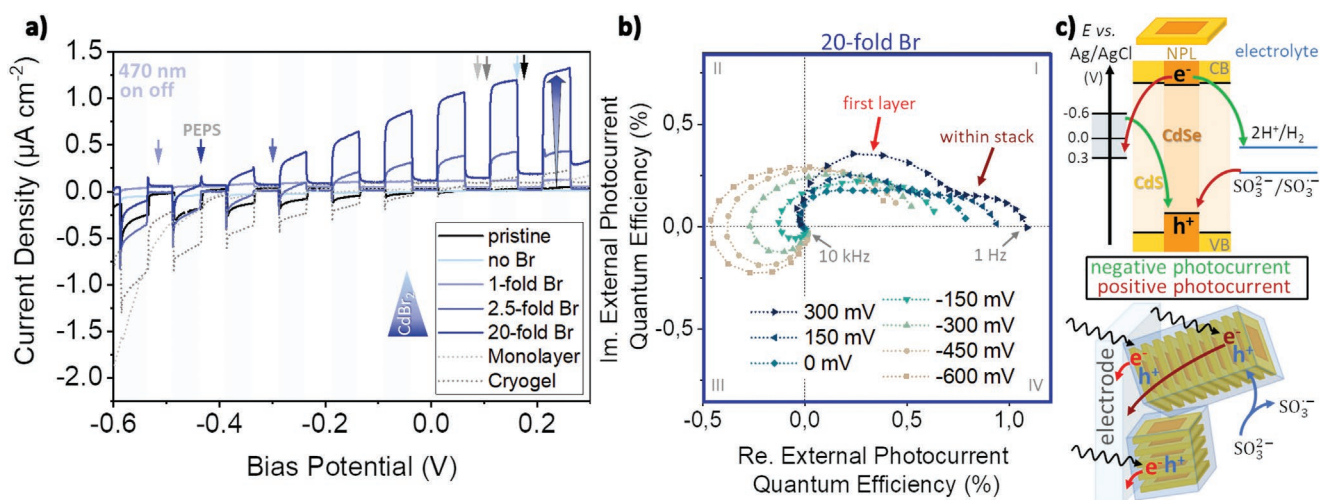


Figure 6. Photo-electrochemical measurements of different PENS: a) linear sweep voltammetry for the different PENS on ITO-glass slides after 24 h (the photo-electrochemical switching point (PEPS) is visualized by arrows) and b) intensity modulated photocurrent spectroscopy of CdSe/CdS-DAm and 20-fold Br PENS after 93 h for different bias potentials. c) Visualization of possible charge carrier transport processes (top). Processes leading to negative photocurrents are symbolized by green arrows and those leading to positive photocurrents by red arrows. c) Possible charge carrier transfer processes in NPL stacks (bottom). (The literature band levels can be found in Figure S25, Supporting Information).

of pristine NPLs, the current density of the PENS sample with the smallest NPL–NPL distance (DAM and 20-fold Br) is significantly higher. This is at first surprising, as in case of PENS the photocurrent density will be damped due to the non-conducting nature of the polymer. However, the (sub-)monolayer electrode will be characterized by a significantly lower coating density, as higher amounts of NPLs can be immobilized if assembled as PENS. Hence, the much higher amount of NPLs seems to be the reason for the higher photocurrent density in case of PENS. An LSV for an electrode coated with a multilayer of NPLs as well as a short characterization of the transients is shown in Figure S31, Supporting Information.

For additional comparison, a randomly ordered system of the building blocks, a so-called cryoaerogel, was prepared. Cryoaerogels consisting of CdSe NPLs have been described before with regards to their optical and photo-electrochemical properties.^[26] If compared to a cryoaerogel containing at least the same CdSe/CdS NPL amount, PENS with small NPL–NPL distances show significantly higher photocurrent densities especially at high bias potentials. The cryoaerogel electrode shows mostly negative photocurrents in the whole potential range. Partially, this is related to the applied high pH (9) of the electrolyte solution, as the PEPS is expected to move to higher bias potentials with rising pH.^[26] However, due to the fact that the pH was kept constant for all investigated systems, differences in the photocurrent amount will be related to differences in the charge carrier dynamics between PENS and cryoaerogels.

In order to investigate the charge carrier dynamics in the different systems more in depth, intensity modulated photocurrent spectra (IMPS) were measured. During an IMPS measurement, the light is modulated with a sine wave function in the frequency range from 10 000 to 1 Hz while a constant bias potential is applied. In Figure 6b, the IMPS of the PENS with lowest NPL–NPL distance (DAM and 20-fold Br) at different bias potentials after 93 h are displayed as Nyquist plots. At low bias potentials (–600 to –150 mV), the IMPS signal starts in the negative photocurrent regime (II and III), thus the e^- transfer to protons and from the electrode to the valence band outperforms the charge carrier recombination. Independent of the bias potential, a turnover from negative to positive photocurrent is observed at high to medium frequencies. This feature is related to the differences in the rate constants of processes leading to negative and positive photocurrents and their predominance depending on the bias potential. As positive photocurrents become dominant at high bias potentials, the turnover point is shifted towards higher frequencies with increasing bias potential.

For bias potentials above –150 mV, two semicircles can be distinguished in the Nyquist plot. The semicircle located in the high frequency range (10 000–63 Hz) can be assigned to the direct transfer of electrons from the first particle layer to the electrode (Figure 6c, bottom, light red arrow). Adjacent to the first semicircle, another semicircle is visible at lower frequencies (63–1 Hz). This can be assigned to electrons generated further away from the electrode surface, which require some time to travel through the NPL assembly in order to reach the electrode (Figure 6c, bottom, dark red arrow).^[24,26] With increasing bias potential, the contribution of negative photocurrents in the high frequency range is drastically decreasing. Furthermore,

the radius of the first semicircle is increasing if moving toward extremely low and high bias potentials, respectively. Both observations are related to the preference of distinct charge transfer processes at certain bias potentials as shown in Figure 6c. The second semicircle, however, seems to be nearly not influenced by the applied bias potential. Hence, the ratio between the first and the second semicircle is decreasing with increasing bias potential (starting at –150 mV). This is in strong contrast to the IMPS response of NPL cryoaerogels, where the percentage of the second semicircle was observed to increase with the bias potential.^[26] The observed differences could be interpreted as follows: while the charge carrier transport in the cryoaerogel requires the bias potential as driving force for the transport and thus, increases with increasing potential, the transport in the PENS with the smallest NPL–NPL distance (DAM and 20-fold Br) seems to be independent from the potential as a driving force. This emphasizes the fast transport of charge carriers through the PENS caused by the small distances. However, due to very low photocurrents for PENS with higher NPL–NPL distances (pristine NPLs and NPLs exchanged with low CdBr₂ amounts), IMPS were not measurable in a sufficient quality.

Furthermore, impedance measurements at 300 mV were conducted to further investigate the influence of the NPL–NPL distance on the PEC properties of the PENS. The impedance spectra (Figure S30, Supporting Information) show that the resistance is smaller for PENS with low NPL–NPL distances (more CdBr₂ in the ligand exchange). The resistance of the system depends on many different barriers which need to be overcome, that is, the barrier between ITO/MPTMS-electrolyte, ITO/MPTMS-polymer-NPL, NPL-polymer-electrolyte, NPL–NPL. Compared to NPL (sub-)monolayer coated electrodes, the resistance increases due to the insulating polymer PMAO. Nevertheless, the transfer is still possible either by tunneling of charge carriers through the organic insulating layer or via regions with incomplete polymer shells.^[24] In all stack syntheses the same amount of insulating polymer was applied, hence the resistance for the contact between the electrode and electrolyte should be comparable for all PENS. Consequently, a smaller resistance of the system could be attributed to the enhanced transport ability that is, smaller resistance within the PENS. This is in good agreement with the results of the LSV and IMPS measurements, in which an enhanced transport through the PENS with smaller NPL–NPL distances (lower tunneling barrier) was observed.

In brief, enhanced electronic transport within PENS with small inter-NPL distances could be verified by different PEC techniques. In the IMPS, it could be distinguished between charge carriers generated close to the electrode and charge carriers which are transported through the PENS. As the contribution of the latter seems to be independent of a driving force (bias potential), simplified charge carrier transport can be concluded for PENS with small inter-NPL distances.

3. Conclusion

To summarize, the synthesis and characterization of different heterostructured polymer encapsulated nanoplatelet stacks (PENS) with to the best of our knowledge unprecedented low

inter-particle distance was shown. PENS with various distances were synthesized. Additionally, extremely small NPL–NPL distances were achieved by applying a ligand exchange with CdBr_2 and amines prior to the stacking and polymer encapsulation steps. It was furthermore shown, that not only the length of the amine but also the applied amount of CdBr_2 plays a crucial role for the resulting NPL–NPL distance in the PENS. The higher the CdBr_2 amount the smaller the resulting NPL–NPL distance in the PENS. By application of different analytical techniques, a competition mechanism between the amine bound as L-type ligand via the lone electron pair of the N and bromide ions bound as X-type ligands could be proposed. This would explain the observed relation between CdBr_2 amount and NPL–NPL distance, as a lower amine density would cause less steric hindrance, leading to less stretched ligands on the surface and thus, a better intercalation with smaller distances between the neighboring NPLs. Additionally, it was shown that the ligand exchange is highly beneficial for the stacking ability of NPLs, what enabled the formation of PENS out of NPLs with very poor stacking behavior (e.g., CdSe/CdS core/shell NPLs).

Through (photo-)electrochemical measurements, the benefit of smaller distances for the charge carrier transport was indicated by much higher photocurrent densities. Furthermore, the IMPS showed a bias-independent electron transport through the PENS for the smallest NPL–NPL distance. Whether the charge carriers are transported by homo-FRET or, more probably, by electron tunneling, provides a vast of unexplored potential to be investigated in the future and which could be addressed through terahertz spectroscopy for the different NPL–NPL distanced samples.

4. Experimental Section

Reagents: Sodium myristate ($\geq 99\%$), methanol (MeOH, $\geq 99.8\%$), 1-octadecene (ODE, 90%), *n*-hexane ($\geq 99\%$), cadmium bromide tetrahydrate (CdBr_2 , 98%), cadmium chloride (CdCl_2 , 99.99%), dodecylamine (DAM, $\geq 99\%$), tetradecylamine (TdAm, 95%), poly(maleic anhydride-*alt*-1-octadecene) (PMAO, M_n 30–1000–50–1000), 1-octanethiol (98.5%), and ethanol (EtOH, $\geq 99.8\%$) were purchased from Sigma Aldrich. Cadmium nitrate tetrahydrate (99.999%), selenium (99.999%), decanoic acid (DAC, 99%) and oleic acid (OlAc, 90%) were supplied by Alfa Aesar. Cadmium acetate dihydrate ($\text{Cd}(\text{Ac})_2$, 98%), tellurium (99.999%), octanoic acid (98%), and tri-*n*-octyl phosphine (TOP, 97%) were purchased from ABCR. Tetrahydrofuran (THF, extra dry, 99.5%), acetonitrile (ACN, extra dry, 99.9%), and oleylamine (OlAm, 80–90%) were supplied by Acros. All chemicals were used as received without further purification.

Synthesis of CdSe Core NPLs: CdSe core NPLs with a quasi-quadratic shape were synthesized following a procedure previously published in literature.^[24,34]

Synthesis of CdSe/CdS Core/Crown NPLs: CdS crowns on CdSe core NPLs were obtained by following a slightly modified procedure published lately.^[11] At first, ODE (8 mL), OlAc (180 μL), $\text{Cd}(\text{Ac})_2$ (96 mg), and the CdSe NPLs in hexane (1.165 mL, $c_{\text{Cd}}=40 \text{ mmol L}^{-1}$) were combined in a 25 mL three-neck flask. The hexane was carefully removed in vacuum and the mixture was further degassed in vacuum for 45 min at 60 °C. Subsequently, the solution was heated to 240 °C under an Ar atmosphere. When a temperature of 215 °C was reached, a solution of sulfur in TOP (200 μL , 1 M) and ODE (3.8 mL) was injected at a rate of 12 mL h^{-1} . After completion of the injection, the heating mantle was removed and the solution was quickly cooled down to room temperature. The CdSe/CdS NPLs were collected by addition of hexane

(5 mL) and EtOH (7.5 mL), followed by centrifugation (4226 rcf, 10 min). The NPLs were stored in hexane under ambient conditions.

Synthesis of CdSe/CdTe Core/Crown NPLs: CdSe/CdTe core/crown NPLs were synthesized according to the procedure described in literature with slight modifications.^[6] Briefly, ODE (8 mL), OlAc (180 μL), $\text{Cd}(\text{Ac})_2$ (96 mg) and the CdSe NPLs in hexane (1.165 mL, $c_{\text{Cd}}=40 \text{ mmol L}^{-1}$) were loaded into a 25 mL three-neck flask and the hexane was removed in vacuum. The mixture was furthermore degassed in vacuum for 45 min at 60 °C and then heated to 215 °C under an Ar atmosphere. When the reaction temperature was reached, 3 mL of a solution of telluride in TOP (100 μL , 1 M) in ODE (3.9 mL) were injected at a rate of 8 mL h^{-1} . Afterward, the solution was held at the reaction temperature for additional 15 min. Subsequently, the reaction mixture was cooled to room temperature and hexane (5 mL) and EtOH (7.5 mL) were added. After centrifugation at 4226 rcf for 10 min, hexane (5 mL) was added and the mixture was centrifuged again (4226 rcf, 10 min). The supernatant was collected and stored in the dark. The solution of telluride in TOP (1 M) was synthesized according to the already published procedure.^[6]

Synthesis of CdSe/CdS Core/Shell NPLs: Core/shell CdSe/CdS NPL were synthesized with a slightly varied synthesis route from literature.^[7] Thereby, $\text{Cd}(\text{Ac})_2$ (106.7 mg), ODE (10 mL), OlAc (278 μL), and CdSe NPL solution in hexane (438 μL , $c_{\text{Cd}}=39.4 \text{ mmol L}^{-1}$) were degassed for 15 min at room temperature, 40 min at 60 °C and 70 min at 80 °C. After the addition of OlAm (2 mL, from the glove box (GB)) the flask was heated to 300 °C under Ar flow. At 180 °C 6 mL of a 1-octanethiol/ODE solution (98 μL in 7 mL) was injected with a rate of 3 mL h^{-1} . Aliquots were taken after certain injection amounts (2 and 4 mL). Directly after the injection stop the reaction vessel was cooled to room temperature and the product was collected through selective centrifugation. Namely, hexane (10 mL) and EtOH (10 mL) were added and the brown mixture was centrifuged (4226 rcf, 10 min). The precipitate was redispersed in hexane (5 mL) and centrifuged (4226 rcf, 10 min). The red supernatant was centrifuged again to get rid of remaining CdO impurities. The pink fluorescent supernatant was stored in the dark.

Ligand Exchanges with CdBr_2 and Amine: Ligand exchange procedures with different amines (DAM, TdAm, OlAm) and varied amounts of CdBr_2 (or CdCl_2) were performed according to a literature procedure^[8] with slight modifications. Briefly, DAM (80 μL) and a certain amount of a 50 mM solution of CdBr_2 (or CdCl_2) in MeOH (e.g., 198 μL to obtain a 10-fold excess to the amount of Cd surface atoms) were mixed with toluene (6 mL) and shaken for 24 h at room temperature. Afterward, as little MeOH as possible was added to destabilize the NPLs and the mixture was centrifuged at 4226 rcf for 10 min. Finally, the NPLs were redispersed in THF.

Ligand Exchanges with Decanoic Acid: As control experiment a ligand exchange with decanoic acid was performed analogue to the exchange with decyl amine and without CdBr_2 . A CdSe/CdS NPL dispersion in hexane (62 μL , $c_{\text{Cd}} = 52 \text{ mmol L}^{-1}$) was shaken with decanoic acid (63.5 mg) in toluene (3 mL) for ≈ 24 h at room temperature. The NPLs were collected through centrifugation at 2817 rcf for 10 min and redispersed in THF.

Synthesis of PENS: The assembly of the NPLs and the subsequent polymer coating was performed according to a procedure described in the literature with a slight modification.^[24] To a NPL solution in dry THF (150 μL , $c_{\text{Cd}} = 19.57 \text{ mmol L}^{-1}$), which was shaken in an orbital shaker at 340 rpm, dry ACN (400 μL) was added at a rate of 6 mL h^{-1} . After 10 min, a polymer solution (PMAO, 1.32 mg L^{-1}) in THF (210 μL) and ACN (90 μL) was injected (3 mL h^{-1}). 4 min later ACN (500 μL) was introduced with a rate of 6 mL h^{-1} . Water (50 μL) was injected after 2 min and 2 min later the reaction was centrifuged (1409 rcf, 10 min). THF (1 mL) was added to the precipitate and centrifuged again (1409 rcf, 10 min). Afterward, the PENS were redispersed in aqueous or methanolic KOH (pH 9, $1 \times 10^{-5} \text{ M}$).

MPTMS Functionalized Electrodes: For all electrical measurements MPTMS functionalized ITO-glass electrodes were used. The coating was performed according to literature.^[26] First, the ITO/glass electrodes were cleaned with H_2O_2 and NH_3 at 70 °C for 2 h (1:1:5, $\text{H}_2\text{O}_2:\text{NH}_3:\text{H}_2\text{O}$). After rinsing with distilled water and drying, they were functionalized

with MPTMS (1 vol%) through stirring in toluene (60 mL) and MPTMS (600 μL) at 50 °C for 2 h. After rinsing with toluene they were dried and stored in an oven (80 °C) until usage.

PENS Electrodes: To measure PENS in the electrochemical setup, coated electrodes were synthesized and stored under argon atmosphere. The synthesized PENS in methanolic KOH were filled into a rectangular PMMA cylinder glued through silicon on top of the MPTMS coated ITO slides. After evaporation of the solvent the cylinder and silicon was removed carefully, yielding a thin 1 cm \times 1 cm PENS coating.

Cryoaerogel Electrodes: For comparison cryoaerogel electrodes were synthesized by an already published method.^[26,57,58] Namely, the NPLs were phase transferred with MUA followed by coating of a 1 cm \times 1 cm square on a MPTMS-functionalized ITO electrode with a NPL solution (20 μL , 60 mmol L^{-1}) in KOH (0.01 M).^[26] The cryoaerogel was synthesized through rapid freezing in isopentane (−160 °C) and stored in liquid nitrogen over night and afterward in a freezer where it was stored until usage for the electrochemistry.^[58]

Monolayer and Multilayer Electrodes: Through shaking of a MPTMS coated electrode in hexane (10 mL) with a NPL solution (100 μL , 58.8 mmol L^{-1}) over a few days monolayer electrodes were prepared. By prolonging the time multilayer electrodes were achieved. Afterward, the glass side of the ITO-glass slide was wiped clean with toluene.

UV-vis and Photoluminescence Spectroscopy: UV-vis extinction spectra were recorded with a DualFL from Horiba Scientific in quartz cuvettes (path length 1 cm). Photoluminescence (PL) emission and excitation spectra were recorded similarly. PLQY were recorded in absolute mode with the same instrument equipped with a Quanta-Phi integrating sphere. The samples were diluted in the according solvents. For measurements under inert gas a measurement setup in a glove box (Ar atmosphere) with fiber glass optics was connected to the DualFL.

UV-vis absorption spectra were measured at a Agilent Cary 5000 UV-vis-NIR spectrophotometer equipped with an Agilent DRA-2500 integrating sphere. The center-mount position in the sphere was used for all measurements.

Photoluminescence Lifetime Measurements: At a FluoroMax-4 from Horiba Scientific equipped with a FluoroHub time-correlated single photon counting (TCSPC) unit PL lifetime measurements were performed in quartz cuvettes. The samples were excited with a LED light source (454 nm, 1.2 ns pulse width). For shorter lifetimes, an Edinburgh FLS 1000 spectrometer was used. Here, the samples were excited by an Edinburgh EPL pulsed laser (445.1 nm, 80 ps pulse width).

Atomic Absorption Spectroscopy: To determine the Cd ion concentration atomic absorption spectroscopy (AAS) was applied. For the AAS measurements a Varian AA140 instrument equipped with an air/acetylene (1.5:3.5) flame atomiser was used. After removing the solvents through an air flow, the samples were decomposed with aqua regia over night. The samples were diluted with Milli-Q water (18.2 M Ω cm). By measuring six standard solutions a calibration curve was obtained.

Transmission Electron Microscopy: Transmission electron microscopy (TEM) measurements were carried out to investigate the morphology, size and inter-particle-distance of the NPLs and NPL-polymer-hybrids. A Tecnai G2 F20 TMP from FEI equipped with a 200 kV field emission gun was used for all measurements. The samples were prepared by drop-casting the respective (diluted) solution (10 μL) on carbon-coated copper TEM grids (Quantifoil, 300 mesh).

Energy Dispersive X-ray Spectroscopy: EDX was performed with a JEOL JSM-6700F SEM operated at 2 kV in the energy range of 0–10 keV. The according samples were drop-casted on silicon wafers.

Thermogravimetric Analysis: Thermogravimetric analysis (TGA) were carried out on a Mettler Toledo TGA/DSC 3+ under nitrogen flow. The according NPL solutions in THF were drop-casted into aluminium oxide crucibles until a mass of \approx 1 to 2 mg was reached. The samples were heated with 5 °C min^{-1} from 25 to 1000 °C under nitrogen flow (50 mL min^{-1}).

Nuclear Magnetic Resonance: NMR was carried out to obtain information about the composition of the ligand shell. For the NMR measurements the pristine or ligand-exchanged NPLs were purified by two additional precipitation steps with EtOH or MeOH, respectively. In

an Argon-filled glovebox, the purified NPL solution was transferred to an NMR tube and the solvent was removed completely in vacuum in the glovebox antechamber. After drying, the NPLs were redispersed in THF- d_8 . The measurements were performed at room temperature on a Bruker Ascend spectrometer equipped with an Avance III console and a Prodigy BBFO probe. The instrument was operating at an ^1H frequency of 400 MHz.

X-Ray Photo-Electron Spectroscopy: X-ray photo-electron spectroscopy (XPS) was measured with a SPECS XPS device equipped with a PHIPOBOS 100 analyzer and a MCD-5 detector. A pass energy of 20 eV and an Al K α X-ray beam (excitation source) was applied. The according sample solutions were drop-casted onto a Si substrate and dried in a glove box under argon. The analysis was performed using XPSPeakFit 4.1 software.

(Photo-)Electrochemical Measurements: (Photo-)electrochemical measurements were done with a ModuLab XM ECS potentiostat from Solatron, a Hameg HMF 2525 frequency generator from Rohde und Schwarz, and a 7270 general purpose DSP lock-in amplifier from Signal Recovery. As reference electrode a BASi (type RE-5B) Ag/AgCl with a NaCl electrolyte (3 M) was used while a Pt wire was taken as counter electrode. The samples were prepared on functionalized ITO glass electrodes through drying under Ar atmosphere. In our self-build measurement cell^[25] a circle with a diameter of 5 mm (0.2 cm^2) of the working electrode was in touch with the electrolyte, here degassed Na_2SO_3 (0.5 M, pH 9). Two different photo-electrochemical measurements, linear sweep voltammetry and intensity modulated photocurrent spectra, were performed with a 468 nm LED shining from the backside of the ITO-sample electrodes.

Linear Sweep Voltammetry: Linear sweep voltammetry (LSV) was carried out with alternation on-off illumination cycles of each 12.5 s. To gain this the LED was powered with square wave pulses with a periodic time of 25 s. The sweep velocity was 4 mV s^{-1} . A potential range from −600 to 300 mV was chosen to eliminate reduction of the ITO and NPLs (below −650 mV) and oxidation of the NPLs (above 300 mV). Before each measurement a constant potential of −600 mV was applied for 30 s to reach an equilibrium state in the system.

Intensity Modulated Photocurrent Spectra: Intensity modulated photocurrent spectra (IMPS) were performed for different bias potentials between −600 and 300 mV. The LED was alternated with a certain frequency which was modulated between 10 000 and 1 Hz. (The measurement setup is visualized in Figure S26, Supporting Information)

Impedance Spectroscopy: Impedance spectroscopy was measured without light excitation. The potential was kept constant at a certain bias potential while the direction of the circuit was changed with a frequency modulated between 100 000 to 0.1 Hz.

Statistical Analysis: All emission, extinction, and excitation spectra had been normalized to the emission maximum or the maximum of the heavy-hole–electron transition of CdSe, respectively. For measurements derived from TEM images, the mean value with standard derivation together with the number n measured can be found in the according tables. The EDX data was normalized to the sulfur or cadmium signal (when no sulfur was present) as written in the Figure captions for better comparability. XPS measurements were normalized to a value of the background which can be found in the according Figure captions. PL-lifetime measurements were fitted using exponential decay functions following type

$$y = A_1 \times e^{-\frac{x}{\tau_1}} + A_2 \times e^{-\frac{x}{\tau_2}} + A_3 \times e^{-\frac{x}{\tau_3}} + \gamma_0 \quad (1)$$

with the software Origin.

Supporting Information

Supporting Information is available from the Wiley Online Library or from the author.

Acknowledgements

R.T.G. and A.S. contributed equally to this work. N.C.B. thanks the European Research Council (ERC) for financial support under the European Union's Horizon 2020 research and innovation program (grant agreement 714429). Furthermore, this work was supported by the German Research Foundation (Deutsche Forschungsgemeinschaft, DFG) under Germany's excellence strategy within the cluster of excellence PhoenixD (EXC 2122, project ID 390833453). R.T.G. and A.S. thank the Hannover School for Nanotechnology (HSN) for funding. D.Z. acknowledges the program financed by the National Research, Development, and Innovation Office of the Ministry for Innovation and Technology, Hungary (TKP2021-NKTA-05). The authors are thankful to the Laboratory of Nano and Quantum Engineering (LNQE) for providing the TEM facilities and Jürgen Caro and Armin Feldhoff for the SEM-EDX facilities. Additionally, the authors are grateful to Frank Steinbach for the SEM cross-section measurements. Furthermore, the authors would like to thank Jörg Fohrer and the whole NMR department of the Institute of Organic Chemistry at Leibniz Universität Hannover for the NMR measurements.

Open access funding enabled and organized by Projekt DEAL.

Conflict of Interest

The authors declare no conflict of interest.

Data Availability Statement

The data that support the findings of this study are available from the corresponding author upon reasonable request.

Keywords

charge carrier transport, distance variation, ligand exchange, nanoplatelets, photo-electrochemistry, self-assembly, stacks

Received: December 9, 2021

Revised: February 9, 2022

Published online:

- [1] S. Ithurria, B. Dubertret, *J. Am. Chem. Soc.* **2008**, *130*, 16504.
- [2] A. Riedinger, F. D. Ott, A. Mule, S. Mazzotti, P. N. Knüsel, S. J. Kress, F. Prins, S. C. Erwin, D. J. Norris, *Nat. Mater.* **2017**, *16*, 743.
- [3] S. Ithurria, G. Bousquet, B. Dubertret, *J. Am. Chem. Soc.* **2011**, *133*, 3070.
- [4] S. Ithurria, M. D. Tessier, B. Mahler, R. P. Lobo, B. Dubertret, A. L. Efron, *Nat. Mater.* **2011**, *10*, 936.
- [5] M. D. Tessier, C. Javaux, I. Maksimovic, V. Lorette, B. Dubertret, *ACS Nano* **2012**, *6*, 6751.
- [6] M. Dufour, V. Steinmetz, E. Izquierdo, T. Pons, N. Lequeux, E. Lhuillier, L. Legrand, M. Chamorro, T. Barisien, S. Ithurria, *J. Phys. Chem. C* **2017**, *121*, 24816.
- [7] A. A. Rossinelli, A. Riedinger, P. Marqués-Gallego, P. N. Knüsel, F. V. Antolinez, D. J. Norris, *Chem. Commun.* **2017**, *53*, 9938.
- [8] M. D. Tessier, P. Spinicelli, D. Dupont, G. Patriarche, S. Ithurria, B. Dubertret, *Nano Lett.* **2014**, *14*, 207.
- [9] T. K. Kormilina, S. A. Cherevko, A. V. Fedorov, A. V. Baranov, *Small* **2017**, *13*, 1702300.
- [10] S. Ithurria, D. V. Talapin, *J. Am. Chem. Soc.* **2012**, *134*, 18585.
- [11] A. Schlosser, R. T. Graf, N. C. Bigall, *Nanoscale Adv.* **2020**, *2*, 4604.
- [12] Y. Kelestemur, B. Guzelturk, O. Erdem, M. Olutas, T. Erdem, C. F. Usanmaz, K. Gungor, H. V. Demir, *J. Phys. Chem. C* **2017**, *121*, 4650.
- [13] Y. Kelestemur, B. Guzelturk, O. Erdem, M. Olutas, K. Gungor, H. V. Demir, *Adv. Funct. Mater.* **2016**, *26*, 3570.
- [14] S. Pedetti, S. Ithurria, H. Heuclin, G. Patriarche, B. Dubertret, *J. Am. Chem. Soc.* **2014**, *136*, 16430.
- [15] F. Rajadell, J. I. Climente, J. Planelles, *Phys. Rev. B* **2017**, *96*, 035307.
- [16] M. D. Tessier, B. Mahler, B. Nadal, H. Heuclin, S. Pedetti, B. Dubertret, *Nano Lett.* **2013**, *13*, 3321.
- [17] B. Mahler, B. Nadal, C. Bouet, G. Patriarche, B. Dubertret, *J. Am. Chem. Soc.* **2012**, *134*, 18591.
- [18] M. Dufour, J. Qu, C. Greboval, C. Méthivier, E. Lhuillier, S. Ithurria, *ACS Nano* **2019**, *13*, 5326.
- [19] S. Jana, T. N. Phan, C. Bouet, M. D. Tessier, P. Davidson, B. Dubertret, B. Abécassis, *Langmuir* **2015**, *31*, 10532.
- [20] S. Jana, M. de Frutos, P. Davidson, B. Abécassis, *Sci. Adv.* **2017**, *3*, 9e1701483.
- [21] J. L. Mohanan, I. U. Arachchige, S. L. Brock, *Science* **2005**, *307*, 397.
- [22] N. C. Bigall, C. Wilhelm, M. L. Beoutis, M. García-Hernandez, A. A. Khan, C. Giannini, A. Sánchez-Ferrer, R. Mezzenga, M. E. Materia, M. A. Garcia, F. Gazeau, A. M. Bittner, L. Manna, T. Pellegrino, *Chem. Mater.* **2013**, *25*, 1055.
- [23] C. Ziegler, A. Wolf, W. Liu, A. K. Herrmann, N. Gaponik, A. Eychmüller, *Angew. Chem., Int. Ed.* **2017**, *56*, 13200.
- [24] J. F. Miethe, A. Schlosser, J. G. Eckert, F. Lübke, N. C. Bigall, *J. Mater. Chem. C* **2018**, *6*, 10916.
- [25] J. F. Miethe, F. Lübke, J. Poppe, F. Steinbach, D. Dorfs, N. C. Bigall, *ChemElectroChem* **2018**, *5*, 175.
- [26] A. Schlosser, L. C. Meyer, F. Lübke, J. F. Miethe, N. C. Bigall, *Phys. Chem. Chem. Phys.* **2019**, *21*, 9002.
- [27] F. Lübke, J. F. Miethe, F. Steinbach, P. Rusch, A. Schlosser, D. Zámbo, T. Heinemeyer, D. Natke, D. Zok, D. Dorfs, N. C. Bigall, *Small* **2019**, *15*, 1902186.
- [28] D. Zámbo, A. Schlosser, P. Rusch, F. Lübke, J. Koch, H. Pfnür, N. C. Bigall, *Small* **2020**, *16*, 16.
- [29] P. Rusch, D. Zámbo, N. C. Bigall, *Acc. Chem. Res.* **2020**, *53*, 2414.
- [30] S. Naskar, J. F. Miethe, S. Sánchez-Paradinas, N. Schmidt, K. Kanthasamy, P. Behrens, H. Pfnür, N. C. Bigall, *Chem. Mater.* **2016**, *28*, 2089.
- [31] D. Zámbo, A. Schlosser, R. T. Graf, P. Rusch, P. A. Kißling, A. Feldhoff, N. C. Bigall, *Adv. Opt. Mater.* **2021**, *9*, 2170067.
- [32] M. D. Tessier, L. Biadala, C. Bouet, S. Ithurria, B. Abécassis, B. Dubertret, *ACS Nano* **2013**, *7*, 3332.
- [33] B. Guzelturk, O. Erdem, M. Olutas, Y. Kelestemur, H. V. Demir, *ACS Nano* **2014**, *8*, 12524.
- [34] B. Abécassis, M. D. Tessier, P. Davidson, B. Dubertret, *Nano Lett.* **2014**, *14*, 710.
- [35] A. Antanovich, A. Prudnikau, A. Matsukovich, A. Achtstein, M. Artemyev, *J. Phys. Chem. C* **2016**, *120*, 5764.
- [36] R. Momper, H. Zhang, S. Chen, H. Halim, E. Johannes, S. Yordanov, D. Braga, B. Blülle, D. Doblas, T. Kraus, T. Kraus, M. Bonn, H. I. Wang, A. Riedinger, *Nano Lett.* **2020**, *20*, 4102.
- [37] E. Lhuillier, S. Pedetti, S. Ithurria, H. Heuclin, B. Nadal, A. Robin, G. Patriarche, N. Lequeux, B. Dubertret, *ACS Nano* **2014**, *8*, 3813.
- [38] E. Lhuillier, A. Robin, S. Ithurria, H. Aubin, B. Dubertret, *Nano Lett.* **2014**, *14*, 2715.
- [39] E. Lhuillier, S. Ithurria, A. Descamps-Mandine, T. Douillard, R. Castaing, X. Z. Xu, P. L. Taberna, P. Simon, H. Aubin, B. Dubertret, *J. Phys. Chem. C* **2015**, *119*, 21795.
- [40] B. Martinez, C. Livache, N. Goubet, E. Izquierdo, M. G. Silly, S. Ithurria, E. Lhuillier, *Phys. Status Solidi C* **2017**, *14*, 1700138.
- [41] E. Lhuillier, J. F. Dayen, D. O. Thomas, A. Robin, B. Doudin, B. Dubertret, *Nano Lett.* **2015**, *15*, 1736.
- [42] E. Lhuillier, J. F. Dayen, D. O. Thomas, A. Robin, S. Ithurria, H. Aubin, B. Dubertret, *Phys. Status Solidi C* **2016**, *13*, 526.
- [43] A. Robin, E. Lhuillier, X. Z. Xu, S. Ithurria, H. Aubin, A. Ouerghi, B. Dubertret, *Sci. Rep.* **2016**, *6*, 24909.

- [44] J. Qu, P. Rastogi, C. Gréboval, C. Livache, M. Dufour, A. Chu, S. S. Chee, J. Ramade, X. Z. Xu, S. Ithurria, E. Lhuillier, *ACS Appl. Mater. Interfaces* **2020**, *12*, 22058.
- [45] A. Antanovich, A. W. Achtstein, A. Matsukovich, A. Prudnikau, P. Bhaskar, V. Gurin, M. Molinari, M. Artemyev, *Nanoscale* **2017**, *9*, 18042.
- [46] T. Kodanek, H. M. Banbela, S. Naskar, P. Adel, N. C. Bigall, D. Dorfs, *Nanoscale* **2015**, *7*, 19300.
- [47] R. Di Corato, N. C. Bigall, A. Ragusa, D. Dorfs, A. Genovese, R. Marotta, L. Manna, T. Pellegrino, *ACS Nano* **2011**, *5*, 1109.
- [48] C. Tanford, *J. Phys. Chem.* **1972**, *76*, 3020.
- [49] D. Kim, D. C. Lee, *J. Phys. Chem. Lett.* **2020**, *11*, 2647.
- [50] K. Yu, B. Zaman, S. Singh, D. Wang, J. A. Ripmeester, *Chem. Mater.* **2005**, *17*, 2552.
- [51] M. G. Spirin, S. B. Brichkin, V. F. Razumov, *High Energy Chem.* **2015**, *49*, 426.
- [52] M. J. Greaney, E. Couderc, J. Zhao, B. A. Nail, M. Mecklenburg, W. Thornbury, F. E. Osterloh, S. E. Bradforth, R. L. Brutchey, *Chem. Mater.* **2015**, *27*, 744.
- [53] NIST X-ray Photoelectron Spectroscopy Database, NIST Standard Reference Database Number 20 (retrieved [21.04.2021]), National Institute of Standards and Technology, Gaithersburg MD, 20899, **2000**.
- [54] Y.-E. E. Shin, Y. J. Sa, S. Park, J. Lee, K.-H. H. Shin, S. H. Joo, H. Ko, *Nanoscale* **2014**, *6*, 9734.
- [55] W. A. Tisdale, X. Y. Zhu, *Proc. Natl. Acad. Sci. U. S. A.* **2011**, *108*, 965.
- [56] W. Wegscheider, G. Schedelbeck, M. Bichler, G. Abstreiter, *Phys. E* **1998**, *3*, 103.
- [57] D. Müller, D. Zámbo, D. Dorfs, N. C. Bigall, *Small* **2021**, *17*, 2007908.
- [58] D. Müller, L. F. Klepzig, A. Schlosser, D. Dorfs, N. C. Bigall, *Langmuir* **2021**, *37*, 5109.